Large Volume and Fast Response Gamma Ray Diagnostic in the Large Helical Device*)

Kunihiro OGAWA[1,2], Siriyaporn SANGAROON[3] and Mitsutaka ISOBE[1,2]

[1)]*National Institute for Fusion Science, National Institutes of Natural Sciences, Toki 509-5292, Japan*
[2)]*The Graduate University for Advanced Studies, SOKENDAI, Toki 509-5292, Japan*
[3)]*Mahasarakham University, 20 41 Kham Riang, Kantharawichai District, Maha Sarakham 44150, Thailand*

(Received 17 November 2022 / Accepted 7 February 2023)

A large volume and fast response gamma ray diagnostic based on the $LaBr_3$(Ce) scintillator was installed to obtain the gamma ray spectrum in the Large Helical Device (LHD) for understanding energetic ion confinement. The advantages of the $LaBr_3$(Ce) scintillator are relatively sensitive to gamma rays due to its relatively heavy weight density of 5.3 g/cc, high counting operation because of a relatively short pulse width of ~ 100 ns, and relatively better energy resolution of ~3%. The gamma ray diagnostic was installed at the outboard side of LHD. The radiation shielding for the $LaBr_3$(Ce) detector was designed to avoid unwanted signals due to stray neutrons and gamma rays using the three-dimensional radiation transport calculation MCNP6. In-situ energy calibration of the $LaBr_3$(Ce) detector was performed using ^{60}Co and ^{137}Cs gamma ray sources. We surveyed a neutron effect on the $LaBr_3$(Ce) detector in an electron-cyclotron-heated deuterium plasma discharge. The pulse counting rate of $LaBr_3$(Ce) detector under the total neutron emission rate of 2×10^{11} n/s was 110 kcps. Therefore, the $LaBr_3$(Ce) detector is expected to be utilized in most of ion cyclotron resonance frequency (ICRF) discharges, where the total neutron emission rate of $\sim10^{11}$ n/s. We plan to measure the gamma ray spectrum in deuterium ICRF discharges.

Keywords: Large Helical Device, nuclear fusion, $LaBr_3$(Ce) detector, gamma ray diagnostic

DOI: 10.1585/pfr.18.2402016

1. Introduction

Gamma ray spectral diagnostics have been utilized in fusion plasma experimental research because the diagnostics provide important information on understanding the MeV ion confinement. In deuterium (D) or deuterium-tritium (D-T) plasma experiments, gamma ray diagnostics have been developed as ion temperature plasma diagnostics [1] and the complementary energetic ion diagnostics, especially for the MeV range [2–4]. In Tokamak Fusion Test Reactor TFTR, a gamma ray detector [5] was utilized for a D-^{3}He experiment [6, 7], as well as controlling runaway electrons generated by disruption [8]. In Joint European Torus JET, a reconstruction of energetic ion distribution was performed using gamma ray spectrometry in D [9] and D-T experiments [10]. After that, the gamma ray detector was upgraded to be operated under a MHz count rate range to obtain detailed measurements of alpha particle confinement research [11]. In ITER, alpha particle energy distribution [12–14] and loss [15] will be measured employing gamma ray detectors. In DEMO, a gamma ray detector will be utilized to measure fuel temperature and ratio in the plasma core [15–17]. Moreover, in aneutronic fusion, such as D-^{3}He and p-^{11}B, gamma ray diagnostics are the candidate for the fusion power monitor [5, 18]. In the D-^{3}He study in large tokamaks, 16.7 MeV gamma rays due to a ^{3}He(d,γ)^{5}Li reaction have been observed using large volume and relatively heavy gamma ray detectors [19]. In addition to plasma diagnostics utilization, the gamma ray detector has played an important role in radiation management for human safety and research for activation levels after operation [20].

In the Large Helical Device (LHD), gamma ray diagnostics have been mainly utilized to study activation research after plasma discharges [21, 22]. Understanding the distribution and gamma ray spectra after plasma discharge in the vacuum vessel [23] and the torus hall [24] will provide important information for human safety as well as knowledge about machine decommission. Gamma ray diagnostics during a neutral-beam-heated deuterium plasma discharge is regarded as a less important diagnostics compared with integrated neutron diagnostic [25], which can directly provide a beam ion confinement property [26–28] because neutrons are mainly produced by so-called beam-thermal reactions in LHD deuterium plasma experiments [29]. Recently, an ion cyclotron resonance frequency (ICRF) wave-heated deuterium plasma experiment was performed with relatively low-power ICRF-heated deuterium plasma [30]. Gamma ray spectroscopy can provide the energy distribution of MeV range ICRF tail ions in a deuterium plasma experiment. Note that a MeV range ICRF proton tail has been observed in steady-

author's e-mail: ogawa.kunihiro@nifs.ac.jp

*) This article is based on the presentation at the 31st International Toki Conference on Plasma and Fusion Research (ITC31).

state hydrogen plasma discharges in LHD [31]. Moreover, gamma ray diagnostics will play an important role in knock-on tail observation through the ^{6}Li(d,γ)^{8}Be reaction [32] or a study toward aneutronic fusion [33].

2. Setups of Large-Volume and Fast-Response Gamma Ray Diagnostic

2.1 Arrangement

A gamma ray diagnostic characterized by large volume and a fast time response based on a $LaBr_3$(Ce) scintillator is installed on the outboard side diagnostic port, the so-called 8-O port, near LHD, as shown in Fig. 1 (a). The cut view of the gamma ray diagnostic is shown in Fig. 1 (b). A large-volume $LaBr_3$(Ce) detector, a relatively large size $LaBr_3$(Ce) scintillator (3-inch height and 3-inch diameter) directly coupled with a 3.5-inch diameter photomultiplier tube (R10233, Hamamatsu Photonics K. K.), is surrounded by a 10-mm thick steel (SS400) cylindrical magnetic shield box. The $LaBr_3$ scintillator is characterized by a relatively high-time response due to the narrow pulse width (~100 ns) and relatively high sensitivity to gamma rays, owing to the high weight density (5.08 g/cm^3). It is worth noting that the stray magnetic field intensity at the detector position in a high magnetic field condition in LHD, e.g., toroidal magnetic field B_t of 2.75 T, is 30 mT. The $LaBr_3$(Ce) detector is immersed in a 10% borated polyethylene block to reduce the neutron effect [34]. Note that the side and back of the $LaBr_3$(Ce) detector are surrounded by 50 mm thick lead to reduce the stray gamma ray effect. The total weight of the gamma ray diagnostics is approximately 450 kg.

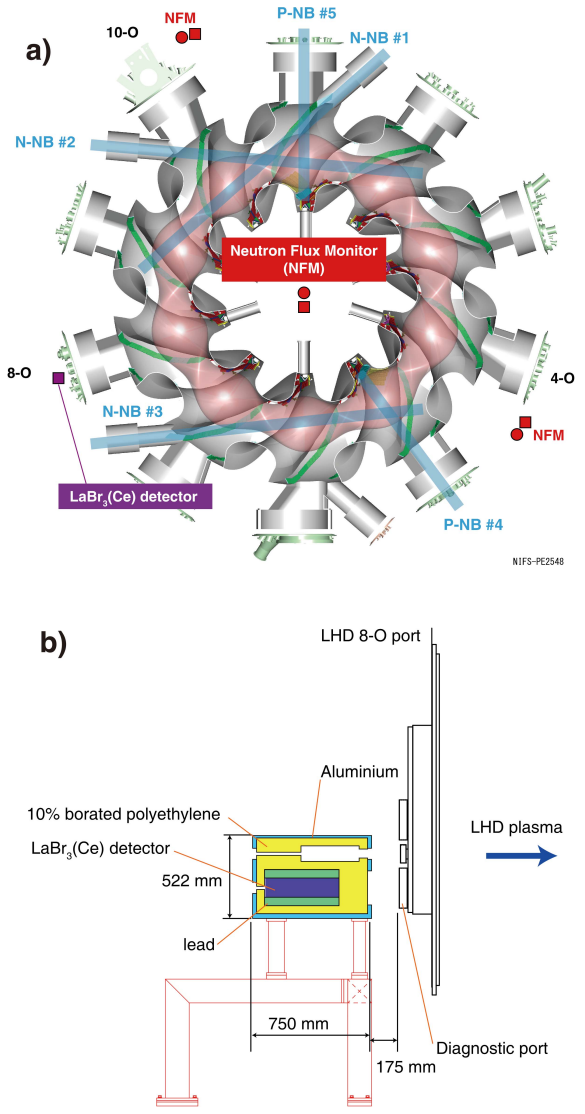

Fig. 1 (a) Bird's eye view of the Large Helical Device. Locations of the $LaBr_3$(Ce) detector and neutron flux monitor. (b) Cut view of radiation shield for the $LaBr_3$(Ce) detector.

2.2 Shielding design

The neutron and gamma ray shielding for the $LaBr_3$(Ce) detector was designed based on the three-dimensional Monte Carlo neutron and gamma ray transport calculation MCNP6 [35]. The most stringent limitation of the shield was that of the allowable weight of the diagnostic stage, 250 kg/m^2. The allowed area for this gamma ray diagnostic is ~2 m^2. Therefore, the total weight should be, at most, 500 kg.

In this calculation, we set a simple torus volume 1.9×10^{16} s^{-1} neutron source with a major radius of 3.6 m and minor radius of 0.6 m. We considered D-D and D-T neutrons with a ratio of 99.5:0.5, according to the maximum obtained secondary triton burnup ratio in LHD [27]. The neutron flux averaged in the $LaBr_3$(Ce) detector was evaluated using an F4 tally. Figure 2 shows a two-dimensional distribution of the neutron and the gamma ray fluxes near the $LaBr_3$(Ce) detector position. The polyethylene shield effectively reduced the neutron flux by two orders of magnitude, and the lead reduced the gamma rays by one order of magnitude.

2.3 Data acquisition and remote-control high voltage system

Figure 3 shows the block diagram of control and data acquisition for gamma ray diagnostic.

The anode signal of the photomultiplier tube of the $LaBr_3$(Ce) detector is transferred with a double shield 50 Ohm 60 m coaxial cable (3D-FB) to the data acquisition system (APV8102-14MWPSAGb, Techno AP), developed for a vertical neutron camera in LHD [36], located at the basement level of LHD torus hall to avoid radiation effects on the system [37]. The data acquisition system consists of a 14-bit 1 GHz sampling analog to digital converter and a field-programmable logic circuit, which realizes online and offline pulse analysis under a MHz pulse counting rate. We performed offline pulse height analysis for $LaBr_3$(Ce) detector signal analysis, using the acquired pulse signals. The acquired data is temporarily stored in

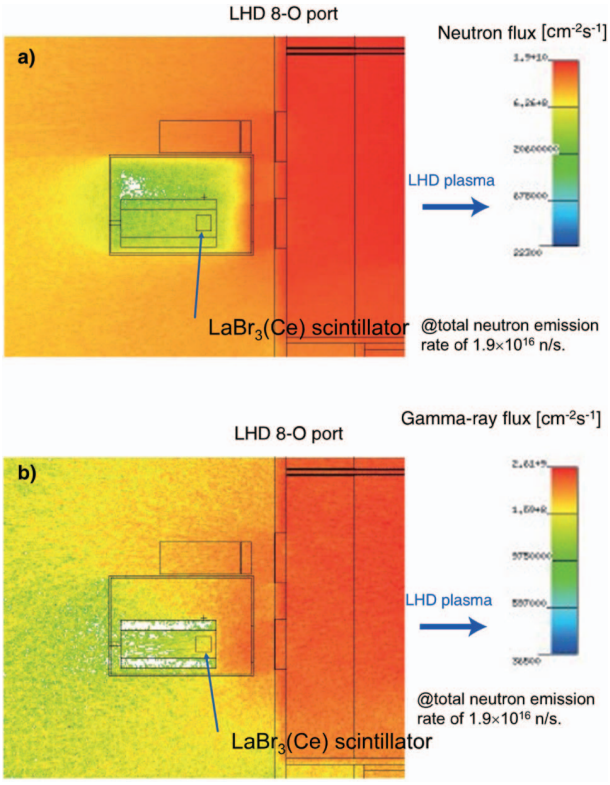

Fig. 2 Result of three-dimensional radiation transport calculation for (a) neutron flux and (b) gamma ray flux at total neutron emission of 1.9×10^{16} n/s.

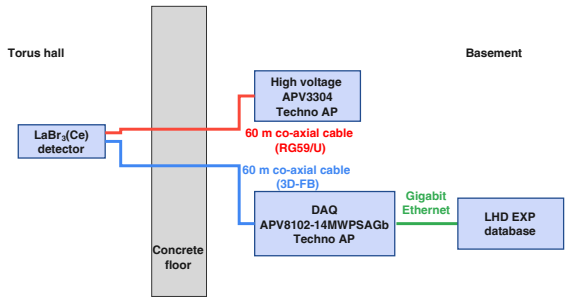

Fig. 3 Block diagram of control and data acquisition for gamma ray diagnostic.

the 1 GB dynamic random-access memory of the data acquisition system and then transferred to the LHD experiment database through the gigabit ethernet at the end of discharge. The high voltage to the $LaBr_3$(Ce) detector 800 V is applied by a 4-ch externally controllable high voltage system (APV3304, Techno AP). The maximum applied voltage is +3 keV, and the maximum output current is 1 mA. We can control the applied high voltage via the LABCOM system [38]. The logging function implemented in the high voltage system allows us to obtain the time evolution of the actual applied voltage and induced current with a 1 ms time bin to monitor the detector's gain variation.

3. Performance of Gamma Ray Diagnostics

3.1 Energy calibration using gamma ray source

In-situ energy calibration of the $LaBr_3$(Ce) detector was performed using ^{137}Cs and ^{60}Co gamma ray calibration sources. The radio activities of the ^{137}Cs and ^{60}Co sources were 0.98 MBq and 0.55 MBq, respectively, on 13th April 2022. Note that ^{137}Cs emitted the 0.662 MeV gamma ray. ^{60}Co emitted 1.173 MeV and 1.332 MeV gamma rays. The gamma ray source was placed on a diagnostics port in front of the detector. The distance from the gamma ray source to the detector was 350 mm. At first, we measured the background pulse height spectrum without a gamma ray calibration source for checking the background gamma ray in the torus hall and the self-radioactivity of Lanthanum. It is well known that Lanthanum has self-radioactivity. It is worth noting that ^{138}La emits 0.788 MeV gamma rays due to beta decay and 1.435 MeV gamma rays due to electronic capture. Figure 4 (a) shows the background pulse height spectrum. The peaks on 0.180 V and 0.327 V seem to correspond to 0.788 MeV and 1.435 MeV, respectively. In the ^{137}Cs source case, we obtained a clear peak at a pulse height of 0.146 V. It was found that the energy resolution, full width at half maximum (FWHM) divided by peak pulse height, for 0.662 MeV was 3.5%. In the ^{60}Co case, we obtained peaks at 0.262 V and 0.298 V. The energy resolutions for 1.173 MeV and 1.332 MeV were 2.8% and 2.4%, respectively. From the relation between pulse height and gamma ray energy shown in Fig. 4 (d), we obtained the calibration factor of gamma rays as (gamma ray energy) [MeV] = 4.4 × (pulse height [V]) + 0.013.

3.2 Neutron effect on the $LaBr_3$(Ce) detector

We performed the experiment to survey the operation limit of the $LaBr_3$(Ce) detector from the aspects of the pulse counting rate, due to a neutron-induced pulse signal under the deuterium plasma discharge. Figure 5 (a) shows the waveform of the discharge. In this discharge, plasma was initiated by electron-cyclotron-resonance heating (ECH) and auxiliary heating by neutral beam (NB) injections. Here, NB2 and NB3 inject hydrogen beams. The time evolution of the $LaBr_3$(Ce) detector counting rate almost follows the time evolution of S_n. In the initial phase, the difference in the time trends might be due to the x-ray effect because the neutron flux monitor, which measures S_n, is insensitive to x-rays. Figure 5 (b) shows the pulse height spectrum obtained from t = 3.3 s to 5.3 s. No clear peak is observed. We found that we can operate this $LaBr_3$(Ce) detector at $S_n \sim 2 \times 10^{11}$ n/s. We can obtain a gamma ray spectrum in most of the deuterium ICRF discharges [39].

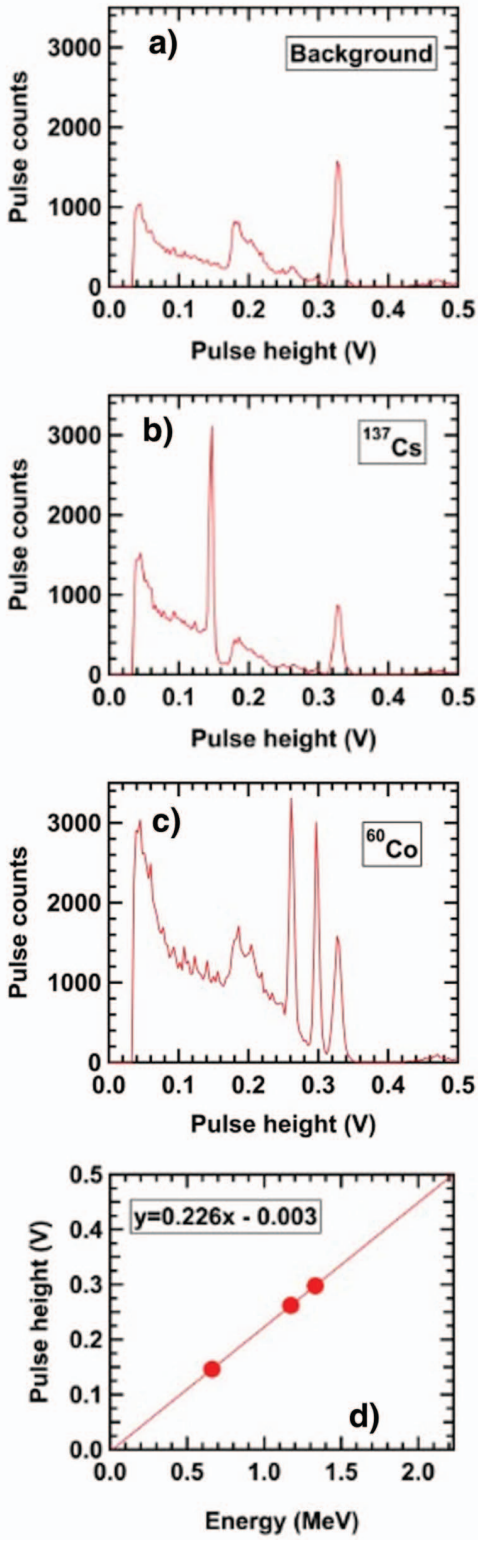

Fig. 4 In-situ energy calibration of $LaBr_3(Ce)$ detector. (a) Background pulse height spectrum. Using ^{137}Cs (b) and ^{60}Co (c) gamma ray sources. (d) Relation between gamma ray energy and pulse height.

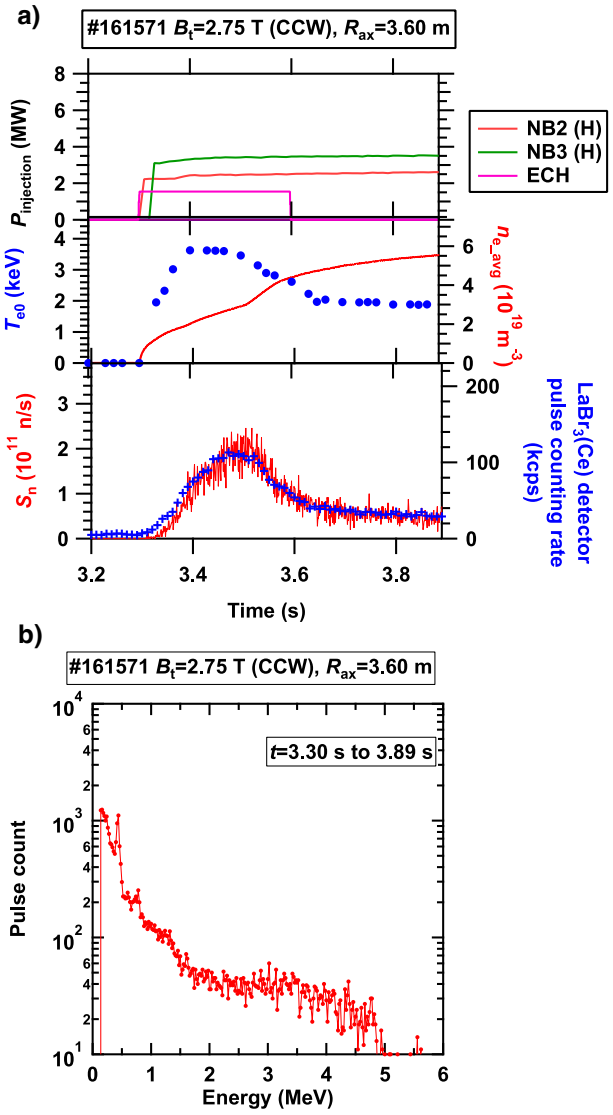

Fig. 5 (a) Time trace of the deuterium plasma discharge. Saturation of pulse counting rate was seen at ~400 kcps. (b) Pulse height spectrum obtained in the experiment. No particular peak is observed.

4. Summary

A large volume and fast response gamma ray diagnostic was installed in the Large Helical Device in order to understand energetic ion confinement study through gamma ray spectrum measurement. The 3-inch diameter and 3-inch height $LaBr_3(Ce)$ detector was characterized by a relatively short decay time (~100 ns), and relatively high-energy resolution was utilized as the gamma ray detector. To reduce the unwanted pulse signal included by fast-neutron and stray gamma rays, the radiation shield composed of 10% borated polyethylene and lead was designed based on a three-dimensional neutron and gamma ray transport calculation by MCNP6. In-situ calibration of the $LaBr_3(Ce)$ detector using gamma ray sources was performed. The unwanted neutron-induced pulse counting rate of the $LaBr_3(Ce)$ detector was measured in an ECH-heated deuterium plasma discharge. We found that the operation of the $LaBr_3(Ce)$ detector will be possible in most of deuterium ICRF discharge because typical expected neutron-induced pulse counts will be at an acceptable level. Also, the diagnostics system might be used to

monitor the activation gamma-ray spectrum after the high-S_n NB-heated discharge.

Acknowledgments

We are pleased to acknowledge the assistance of the LHD Experiment Group.

[1] F.E. Cecil *et al.*, Nucl. Instrum. Meth. **175**, 293 (1980).
[2] S.S. Medley *et al.*, Rev. Sci. Instrum. **56**, 975 (1985).
[3] F.E. Cecil and F.J. Wilkinson, III, Phys. Rev. Lett. **53**, 767 (1984).
[4] V.G. Kiptily *et al.*, Plasma Phys. Control. Fusion **48**, R59 (2006).
[5] S.S. Medley *et al.*, Rev. Sci. Instrum. **61**, 3226 (1990).
[6] F.E. Cecil and S.S. Medley, Nucl. Instrum. Meth. in Physics Research Section A **271**, 628 (1988).
[7] S.S. Medley *et al.*, Rev. Sci. Instrum. **63**, 4857 (1992).
[8] E.D. Fredrickson *et al.*, Nucl. Fusion **55**, 013006 (2015).
[9] A. Shevelev *et al.*, Nucl. Fusion **53**, 123004 (2013).
[10] V.G. Kiptily *et al.*, Phys. Rev. Lett. **93**, 115001 (2004).
[11] M. Nocente *et al.*, Rev. Sci. Instrum. **87**, 11E714 (2016).
[12] I.N. Chugunov *et al.*, Nucl. Fusion **51**, 083010 (2011).
[13] V.G. Kiptily *et al.* Tech. Phys. **43**, 471 (1998).
[14] I.N. Chugunov *et al.*, Instrum. Exp. Tech. **51**, 166 (2008).
[15] V.G. Kiptily *et al.*, Nucl. Fusion **58**, 082009 (2018).
[16] A.J.H. Donné, A.E. Costley and A.W. Morris, Nucl. Fusion **52**, 074015 (2012).
[17] V.G. Kiptily, Nucl. Fusion **55**, 023008 (2015).
[18] F.E. Cecil *et al.*, Rev. Sci. Instrum. **61**, 3223 (1990).
[19] T. Nishitani *et al.*, Rev. Sci. Instrum. **72**, 877 (2001).
[20] L.W. Packer *et al.*, Nucl. Fusion **58**, 096013 (2018).
[21] K. Nishimura *et al.*, Plasma Fusion Res. **3**, S1024 (2008).
[22] T. Nishitani *et al.*, Prog. Nucl. Sci. Technol. **6**, 48 (2019).
[23] S. Yoshihashi *et al.*, Plasma Fusion Res. **17**, 2405096 (2022).
[24] T. Tanaka *et al.*, Plasma Fusion Res. **14**, 3405162 (2019).
[25] M. Isobe *et al.*, IEEE Trans. Plasma Sci. **46**, 2050 (2018).
[26] M. Isobe *et al.*, Nucl. Fusion **58**, 082004 (2018).
[27] K. Ogawa *et al.*, Nucl. Fusion **59**, 076017 (2019).
[28] K. Ogawa *et al.*, Plasma Fusion Res. **16**, 1102023 (2021).
[29] M. Osakabe *et al.*, Fusion Sci. Technol. **72**, 199 (2017).
[30] S. Kamio *et al.*, Nucl. Fusion **62**, 016004 (2022).
[31] T. Muto *et al.*, Nucl. Fusion **47**, 1250 (2007).
[32] H. Matsuura *et al.*, Plasma Fusion Res. **11**, 1403105 (2016).
[33] K. Ogawa *et al.*, Fusion Sci. Technol. **78**, 175 (2022).
[34] C. Cazzaniga *et al.*, Rev. Sci. Instrum. **84**, 123505 (2013).
[35] J.T. Goorley, "MCNP6.1.1-Beta Release Notes", LA-UR-14-24680 (2014).
[36] K. Ogawa *et al.*, Rev. Sci. Instrum. **89**, 113509 (2018).
[37] K. Ogawa *et al.*, Nucl. Fusion **57**, 086012 (2017).
[38] H. Nakanishi *et al.*, Fusion Sci. Technol. **58**, 445 (2010).
[39] R. Seki *et al.*, Plasma Fusion Res. **15**, 1202088 (2020).